INTERNATIONAL JOURNAL FOR NUMERICAL METHODS IN FLUIDS
Int. J. Numer. Meth. Fluids 2006; **51**:235–259
Published online 17 November 2005 in Wiley InterScience (www.interscience.wiley.com). DOI: 10.1002/fld.1115

Numerical study of particulate suspension flow through wavy-walled channels

R. Usha[1,*,†], S. Senthilkumar[2] and E. G. Tulapurkara[2]

[1]*Department of Mathematics, Indian Institute of Technology Madras, Chennai 600 036, India*
[2]*Department of Aerospace Engineering, Indian Institute of Technology Madras, Chennai 600 036, India*

SUMMARY

The particulate suspension flow in a channel whose walls describe a travelling wave motion is examined numerically. A perturbation method is employed and the primitive variables are expanded in a series with the wall amplitude as the perturbation parameter. The boundary conditions are applied at the mean surface of the channel and the first-order perturbation quantities are numerically determined by solving the governing system of ordinary differential equations by shooting technique. The present approach does not impose any restriction on the Reynolds number of the flow and the wave number and frequency of the wavy-walled channel, although it is limited by the linear analysis. The wall shear stress and the positions of flow separation and reattachment points are computed and the influence of the volume fraction density of the particles is examined. The variations of velocity and pressure of the particulate suspension flow with frequency of excitation are also presented. Copyright © 2005 John Wiley & Sons, Ltd.

KEY WORDS: particulate suspension flow; wavy-walled channel; peristaltic motion; shooting technique

1. INTRODUCTION

Flow over wavy boundaries occurs in a variety of physical and biological systems and the physical processes involve interactions between the flow field and the wavy surfaces which produce significant changes in the transport of mass, momentum and energy. In some industrial processes, it is sometimes required to produce a flow through a duct without using internal moving parts. Peristaltic transport is one of the methods which involves fluid transfer and avoids internal moving parts and it employs a duct with flexible walls and consists of

*Correspondence to: R. Usha, Department of Mathematics, Indian Institute of Technology Madras, Chennai 600 036, India.
†E-mail: ushar@iitm.ac.in

Contract/grant sponsor: Council of Scientific and Industrial Research, India
Contract/grant sponsor: Department of Science and Technology

Received 29 March 2003
Revised 4 October 2004
Accepted 18 August 2005

vibrating the walls so as to generate progressive transverse deflection waves. In physiological applications, flow in a channel whose walls are subjected to a wave-like forced excitation has been used to transport blood within small blood vessels or artificial blood devices. In bio-fluid mechanics, flow through wavy passages involving peristaltic motion finds its application in the understanding of mechanisms for localization of atherosclerotic lesions. Also, the flow through wavy boundaries give rise to favourable and adverse pressure gradients due to the surface undulations present in the flow configuration and hence, the resulting flow may be treated as a mechanical system not in equilibrium and which is amenable to control.

Various studies on the flow of Newtonian and non-Newtonian fluids through channels and tubes whose walls are subjected to a wave-like forced excitation (experimental, theoretical as well as computational) have been carried out and these investigations have explored a variety of relevant information [1–9]. The peristaltic motion of a mixture of fluid and solid particles has also been theoretically examined, e.g. by Hung and Brown [10] and Kaimal [11], Srivastava and Srivastava [12] and Misra and Pandey [13]. These studies on peristaltic flows of particulate suspension or two-phase model have either neglected inertia or assumed very slow motion, low frequency and small amplitudes. On the other hand, the present numerical study on the particulate suspension flow through a channel whose walls are subjected to a wave-like forced excitation, has been carried out by including inertia as well as pressure gradient terms. No approximation has been made except for the linerization of the governing equations of particulate suspension model.

The problem of flow of a particulate suspension has attracted the attention of several investigators due to the variety of dynamical phenomena exhibited by it and due to its many applications in industry. The importance of the particulate suspension flow/two-phase flow has led to the development of several theories which are based mainly on either Eulerian approach or the Lagrangian approach. The former treats both phases as continua with interfacial interactions such as drag and heat transfer [14–16]. The latter approach treats only the fluid as a continuum while the particle phase is governed by the kinetic theory [17, 18]. Both the approaches have been successfully applied for the analysis and solution of two-phase flow situations. In the present investigation, a particulate suspension flow through a wavy channel is considered on the basis of a continuum model of a suspension of solid particles in a carrier fluid [15, 19–21]. The constituents are treated as superimposed continua and are described by means of field variables and balance equations, obtained through an averaging procedure over regions containing sufficiently large numbers of solid particles. Separate mass and momentum balance equations for each constituent are written and the momentum equations for each phase are coupled through a fluid–solid interaction force, which is taken to be the classical Stokes drag on a single spherical particle and modified by a factor, accounting for a finite volume fraction of particles, obtained by Tam [22]. The continuum model of particulate suspension flow in the present study is thus formulated using constitutive equations that are representative of the work of several previous investigators and that are used by several authors such as Nayfeh [23], Marble [14], Chamkha [24, 25], Jean and Peddieson [26], Apazidis [27] and many of the references appearing therein.

The purpose of the present work is to obtain a numerical solution of a simple model describing the particulate suspension flow in a channel whose walls are subjected to a wave-like forced excitation. It is felt that a good understanding of models of this kind is necessary before proceeding to more complex types. The present investigation on particulate suspension flow is potentially important and relevant in regard to bio-fluid transport by peristalsis of

muscular contractions in body organs where fluids behave like particle–fluid mixtures, namely chyme in small intestine and blood suspension in arteriole.

2. MATHEMATICAL FORMULATION

A two-dimensional infinite channel of mean width $2d$ (Figure 1), filled with a mixture of small spherical rigid particles in an incompressible Newtonian fluid is considered. The walls of the channel described by $y' = -d + \eta'(x,t)$ and $y' = d - \eta'(x,t)$ are subjected to a travelling wave type of excitation. The equations governing conservation of mass and linear momentum for continuum approach can be expressed as [12, 21, 23, 28, 29]

Fluid phase:

$$(1-C)\rho_f\left[\frac{\partial u'_f}{\partial t'} + u'_f\frac{\partial u'_f}{\partial x'} + v'_f\frac{\partial u'_f}{\partial y'}\right] = -(1-C)\frac{\partial p'}{\partial x'} + (1-C)\mu_s(C)\nabla^2 u'_f + CS(u'_p - u'_f) \tag{1}$$

$$(1-C)\rho_f\left[\frac{\partial v'_f}{\partial t'} + u'_f\frac{\partial v'_f}{\partial x'} + v'_f\frac{\partial v'_f}{\partial y'}\right] = -(1-C)\frac{\partial p'}{\partial y'} + (1-C)\mu_s(C)\nabla^2 v'_f + CS(v'_p - v'_f) \tag{2}$$

$$\frac{\partial}{\partial x'}[(1-C)u'_f] + \frac{\partial}{\partial y'}[(1-C)v'_f] = 0 \tag{3}$$

Particulate phase:

$$C\rho_p\left[\frac{\partial u'_p}{\partial t'} + u'_p\frac{\partial u'_p}{\partial x'} + v'_p\frac{\partial u'_p}{\partial y'}\right] = -C\frac{\partial p'}{\partial x'} + CS(u'_f - u'_p) \tag{4}$$

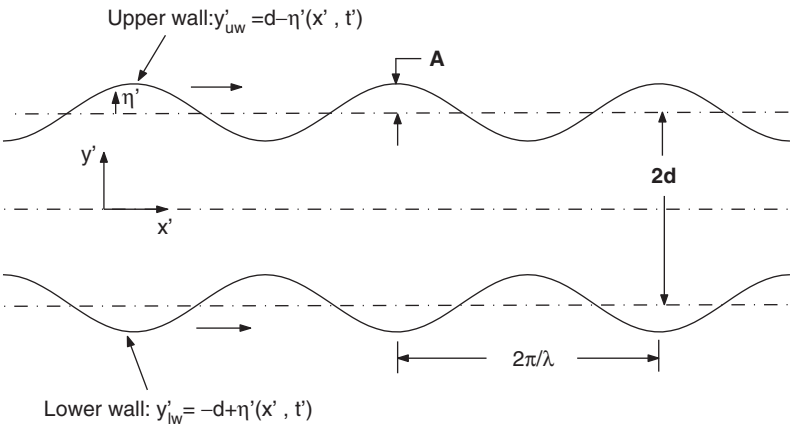

Figure 1. Wavy channel flow configuration.

$$C\rho_{\mathrm{p}}\left[\frac{\partial v'_{\mathrm{p}}}{\partial t'}+u'_{\mathrm{p}}\frac{\partial v'_{\mathrm{p}}}{\partial x'}+v'_{\mathrm{p}}\frac{\partial v'_{\mathrm{p}}}{\partial y'}\right]=-C\frac{\partial p'}{\partial y'}+CS(v'_{\mathrm{f}}-v'_{\mathrm{p}}) \tag{5}$$

$$\frac{\partial}{\partial x'}[Cu'_{\mathrm{p}}]+\frac{\partial}{\partial y'}[Cv'_{\mathrm{p}}]=0 \tag{6}$$

where x', y' are cartesian coordinates with x' measured in the direction of wave propagation and y' measured in the direction normal to the mean position of the channel walls (Figure 1), $(u'_{\mathrm{f}}, v'_{\mathrm{f}})$ denotes fluid-phase velocities, $(u'_{\mathrm{p}}, v'_{\mathrm{p}})$ denotes particulate-phase velocities, $\rho_{\mathrm{f}}, \rho_{\mathrm{p}}$, the actual densities of the materials constituting fluid and particulate phases, respectively, $(1-C)\rho_{\mathrm{f}}$ the fluid density, $C\rho_{\mathrm{p}}$, the particulate-phase density, p' denotes the pressure, C denotes the volume fraction density of the particles, $\mu_{\mathrm{s}}(C)$ is the particle–fluid mixture viscosity and S is the drag coefficient of the interaction for the force exerted by one phase on the other.

It should be pointed out here that the volume fraction density C of the particles has been chosen as a constant. This is a good assumption for flows with low concentration of small particles, e.g. slow filtration. This assumption is necessary to obtain closed form solutions that can be used to check the numerical solutions of the transient problem. There are more elaborate constitutive theories which predict non-uniform particle volume fraction [30, 31]. But obviously, in these cases, it is not possible to obtain exact solutions.

As the concentration of the particle has been considered small, the field interaction between the particles can be neglected. The particle phase viscous effects arise from additional shearing due to high particulate concentrations in solid–fluid system. Physically, as the fluid viscosity represents fluid–fluid interaction, the particle viscosity can be thought of as representing the particle–particle interaction. Mathematically, since the particle cloud is not a continuous system, a continuum description of such a system involves averages over small volume elements and/or small time intervals. The actual variables associated with individual particle will not exactly correspond to those averages. This gives rise to the possibility of transfer of mass, momentum and energy which are not accounted for by the average variables [21, 32]. The resulting momentum transfer can be modelled as viscous in nature. A possible application of this type of flow is in powder industry. In the present investigation, however, the diffusivity term, which models the effects of particle–particle impacts due to the Brownian motion has been neglected due to the assumption that the concentration of the particles is small. It is worth mentioning here that the effects of Brownian motion have been considered by others including Batchelor [33, 34].

Since the particle-phase Reynolds number is assumed to be small, other interaction forces such as the virtual mass force [35], the shear lift force [36] and the spin lift force [37] have been neglected compared to the Stokes' drag forces [27]. It should be noted here that the effects of earth's gravity have been neglected. Soo [38] has shown that, compared with the effects of friction, gravity effects in pipe flow of a suspension are very small and therefore can be neglected.

The expression for the drag coefficient for the present problem has been selected as

$$\begin{aligned} S&=\frac{9}{2}\frac{\mu_0}{a^2}\lambda'(C)\\ \lambda'(C)&=\frac{4+3(8C-3C^2)^{1/2}+3C}{(2-3C)^2}\end{aligned} \tag{7}$$

where μ_0 is the fluid viscosity, and 'a' is the radius of the particle. The classical Stokes' drag for small particle Reynolds number has been represented by relation (7) and it accounts for the finite particulate fractional volume through the function $\lambda'(C)$, obtained by Tam [22]. Although there are several empirical relations connecting the viscosity of the suspension, particle concentration and viscosity of the suspending medium, in the present investigation, the relation

$$\mu_s(C) = \frac{\mu_0}{1 - qC}$$
$$q = 0.070 \exp\left[2.49C + \frac{1107}{T}\exp(-1.69C)\right] \tag{8}$$

where T is the absolute temperature (K), suggested by Charm and Kurland [39] has been used. The viscosity of suspension predicted by this formula has been found to be reasonably accurate up to $C = 0.6$. Charm and Kurland [39] have tested Equation (8) with a cone and plate viscometer and found it to be in agreement within 10 per cent for blood suspension.

The boundary conditions are no-slip at the walls and impermeability of the walls of the channel. They are given by

$$u'_f = 0, \quad v'_f = \frac{\partial \eta'}{\partial t'}, \quad v'_p = \frac{\partial \eta'}{\partial t'} \quad \text{on } y' = \pm d \pm \eta' \tag{9}$$

It may be pointed out that in the absence of the exact form of the boundary conditions to be satisfied by a particle at a surface and the experimental fact that a particle experiences a certain amount of slip at a boundary, the boundary condition given by (9) have been chosen. These boundary conditions seem to give a reasonable solution without any difficulty [16].

Taking reference quantities for length, velocity and pressure as 'd', the mean semi-channel height, 'U', the mean-centre line velocity and $\rho_f U^2$, respectively, the dimensionless variables and parameters are

$$x = \frac{x'}{d}, \quad y = \frac{y'}{d}, \quad \eta = \frac{\eta'}{d}, \quad \varepsilon = \frac{A}{d}, \quad t = \frac{Ut'}{d}$$
$$u_f = \frac{u'_f}{U}, \quad v_f = \frac{v'_f}{U}, \quad u_p = \frac{u'_p}{U}, \quad v_p = \frac{v'_p}{U}, \quad p = \frac{p'}{\rho_f U^2} \tag{10}$$
$$Re = \frac{Ud\rho_f}{\mu_s(C)(1-C)}, \quad M = \frac{Sd^2}{(1-C)\mu_s}$$

The system of Equations (1)–(6) and (9) can now be expressed as

Fluid phase:

$$(1-C)Re\left[\frac{\partial u_f}{\partial t} + u_f\frac{\partial u_f}{\partial x} + v_f\frac{\partial u_f}{\partial y}\right] = -(1-C)Re\frac{\partial p}{\partial x} + \nabla^2 u_f + CM(u_p - u_f) \tag{11}$$

$$(1-C)Re\left[\frac{\partial v_f}{\partial t} + u_f\frac{\partial v_f}{\partial x} + v_f\frac{\partial v_f}{\partial y}\right] = -(1-C)Re\frac{\partial p}{\partial y} + \nabla^2 v_f + CM(v_p - v_f) \tag{12}$$

$$\frac{\partial}{\partial x}[(1-C)u_{\mathrm{f}}]+\frac{\partial}{\partial y}[(1-C)v_{\mathrm{f}}]=0 \tag{13}$$

Particulate phase:

$$C\,Re\left[\frac{\partial u_{\mathrm{p}}}{\partial t}+u_{\mathrm{p}}\frac{\partial u_{\mathrm{p}}}{\partial x}+v_{\mathrm{p}}\frac{\partial u_{\mathrm{p}}}{\partial y}\right]=-C\,Re\frac{\rho_{\mathrm{f}}}{\rho_{\mathrm{p}}}\frac{\partial p}{\partial x}+C\frac{\rho_{\mathrm{f}}}{\rho_{\mathrm{p}}}M(u_{\mathrm{f}}-u_{\mathrm{p}}) \tag{14}$$

$$C\,Re\left[\frac{\partial v_{\mathrm{p}}}{\partial t}+u_{\mathrm{p}}\frac{\partial v_{\mathrm{p}}}{\partial x}+v_{\mathrm{p}}\frac{\partial v_{\mathrm{p}}}{\partial y}\right]=-C\,Re\frac{\rho_{\mathrm{f}}}{\rho_{\mathrm{p}}}\frac{\partial p}{\partial y}+C\frac{\rho_{\mathrm{f}}}{\rho_{\mathrm{p}}}M(v_{\mathrm{f}}-v_{\mathrm{p}}) \tag{15}$$

$$\frac{\partial}{\partial x}[Cu_{\mathrm{p}}]+\frac{\partial}{\partial x}[Cv_{\mathrm{p}}]=0 \tag{16}$$

Boundary condition:

$$u_{\mathrm{f}}=0,\quad v_{\mathrm{f}}=\frac{\partial\eta}{\partial t},\quad v_{\mathrm{p}}=\frac{\partial\eta}{\partial t}\quad \text{on } y=\pm 1\pm\eta \tag{17}$$

The wall motion can be specified through the following expressions:

$$y_{\text{upperwall}}=+1-\varepsilon\ (\text{Real part of } [\exp \mathrm{i}(\lambda x-\omega t)]) \tag{18}$$

$$y_{\text{lowerwall}}=-1+\varepsilon\ (\text{Real part of } [\exp \mathrm{i}(\lambda x-\omega t)]) \tag{19}$$

which represent a wave travelling in the plane of the wall around the position $y=\pm 1$ with amplitude ε, wave number vector $(\lambda,0,0)$ and frequency ω. The wave number of the wavy channel configuration for both top and bottom walls of the channel is same and has been considered to be small, namely, wavelength has been taken to be long as compared to the amplitude, although no such limitation has been imposed by the formulation or the solution technique. When the wave number of the wall is prescribed, then the flow through the channel becomes spatially periodic. When the walls of the channel are subjected to wave excitation, then its circular frequency ω is prescribed. This renders the flow periodic in both temporal and spatial aspects. The amplitude of the wavy motion ε is the same for both top and bottom walls of the channel and is considered small as compared to the width of the channel. It may be pointed out that the case of zero excitation corresponds to a rigid wavy boundary. In the form given by (18) and (19), the waves of the upper and lower walls are in anti-phase, so that at any instant of time, the local channel width expands and contracts around the value $2d$.

In what follows, the flow of a particulate suspension through the channel subjected to wave excitation at the walls has been examined. For small amplitude of wavy-wall excitation, the solution has been sought as a perturbation from the velocity profile of the fully developed channel flow. It is worth mentioning here that, correctors or perturbation parts must be introduced in order to correct the homogeneous boundary conditions on the rough wall which are no longer satisfied by the basic part [40, 41]. To linear approximation in ε, the flow quantities can be expressed as

$$F=\bar{F}(y)+\varepsilon\tilde{F}(x,y,t)+O(\varepsilon^2) \tag{20}$$

where F can be u_f, v_f, u_p or v_p; $\bar{F}$ is the solution for the basic flow and $\tilde{F}$ is for perturbation part. Substituting (20) in (11)–(16) and collecting the terms of different orders in ε, say up to ε^1, the equations for the basic flow and perturbed quantities can be obtained. It is important to note that different formal asymptotic expansion must be used to treat different regimes. The equations determining the basic flow are

$$\begin{aligned} -(1-C)Re\frac{\partial \bar{p}}{\partial x} + \frac{\partial^2 \bar{u}_f}{\partial y^2} + CM(\bar{u}_p - \bar{u}_f) = 0 \\ -Re\frac{\partial \bar{p}}{\partial x} + M(\bar{u}_f - \bar{u}_p) = 0 \end{aligned} \tag{21}$$

The solution of Equation (21) using the boundary condition $\bar{u}_f(\pm 1) = 0$ is

$$\begin{aligned} \bar{u}_f &= k(1-y^2) \\ \bar{u}_p &= k\left(1 - y^2 + \frac{2}{M}\right) \\ \bar{p} &= -\frac{2kx}{Re} \end{aligned} \tag{22}$$

where $k = -Re/2\partial p/\partial x$ is the Poiseuille flow parameter. It may be noted that the effect of the particles on the fluid velocity profile is to cause an increase in the viscosity, that is, the fluid viscosity μ_0 is replaced by suspension viscosity $\mu_s = \mu_0/(1-qC)$ and that for a given pressure difference, less fluid will flow through the channel. Further the particles lead the fluid by a relative velocity proportional to $1/M\partial p/\partial x$.

The perturbed quantities can be obtained from

$$\begin{aligned} (1-C)Re\left[\frac{\partial \tilde{u}_f}{\partial t} + \bar{u}_f\frac{\partial \tilde{u}_f}{\partial x} + \tilde{v}_f\frac{\partial \bar{u}_f}{\partial y}\right] = -(1-C)Re\frac{\partial \tilde{p}}{\partial x} + \nabla^2\tilde{u}_f \\ + CM(\tilde{u}_p - \tilde{u}_f) \end{aligned} \tag{23}$$

$$\begin{aligned} (1-C)Re\left[\frac{\partial \tilde{v}_f}{\partial t} + \bar{u}_f\frac{\partial \tilde{v}_f}{\partial x}\right] = -(1-C)Re\frac{\partial \tilde{p}}{\partial y} + \nabla^2\tilde{v}_f \\ + CM(\tilde{v}_p - \tilde{v}_f) \end{aligned} \tag{24}$$

$$\frac{\partial}{\partial x}[(1-C)\tilde{u}_f] + \frac{\partial}{\partial y}[(1-C)\tilde{v}_f] = 0 \tag{25}$$

$$C\,Re\left[\frac{\partial \tilde{u}_p}{\partial t} + \bar{u}_p\frac{\partial \tilde{u}_p}{\partial x} + \tilde{v}_p\frac{\partial \bar{u}_p}{\partial y}\right] = -C\,Re\frac{\rho_f}{\rho_p}\frac{\partial \tilde{p}}{\partial x} + C\frac{\rho_f}{\rho_p}M(\tilde{u}_f - \tilde{u}_p) \tag{26}$$

$$C\,Re\left[\frac{\partial \tilde{v}_p}{\partial t} + \bar{u}_p\frac{\partial \tilde{v}_p}{\partial x}\right] = -C\,Re\frac{\rho_f}{\rho_p}\frac{\partial \tilde{p}}{\partial y} + C\frac{\rho_f}{\rho_p}M(\tilde{v}_f - \tilde{v}_p) \tag{27}$$

$$\frac{\partial}{\partial x}[C\tilde{u}_p] + \frac{\partial}{\partial y}[C\tilde{v}_p] = 0 \tag{28}$$

To solve Equations (23)–(28), the form of solution, of ε^1 order, can be assumed as

$$\begin{aligned}
\tilde{u}_{\mathrm{f}'} &= \tfrac{1}{2}[\hat{u}_{\mathrm{f}}(y)\exp\{\mathrm{i}(\lambda x-\omega t)\}+\hat{u}_{\mathrm{f}}^{*}(y)\exp\{-\mathrm{i}(\lambda x-\omega t)\}]\\
\tilde{v}_{\mathrm{f}} &= \tfrac{1}{2}\hat{v}_{\mathrm{f}}(y)\exp\{\mathrm{i}(\lambda x-\omega t)\}+\hat{v}_{\mathrm{f}}^{*}(y)\exp\{-\mathrm{i}(\lambda x-\omega t)\}]\\
\tilde{u}_{\mathrm{p}} &= \tfrac{1}{2}[\hat{u}_{\mathrm{p}}(y)\exp\{\mathrm{i}(\lambda x-\omega t)\}+\hat{u}_{\mathrm{p}}^{*}(y)\exp\{-\mathrm{i}(\lambda x-\omega t)\}]\\
\tilde{v}_{\mathrm{p}} &= \tfrac{1}{2}[\hat{v}_{\mathrm{p}}(y)\exp\{\mathrm{i}(\lambda x-\omega t)\}+\hat{v}_{\mathrm{p}}^{*}(y)\exp\{-\mathrm{i}(\lambda x-\omega t)\}]\\
\tilde{p} &= \tfrac{1}{2}[\hat{p}(y)\exp\{\mathrm{i}(\lambda x-\omega t)\}+\hat{p}^{*}(y)\exp\{-\mathrm{i}(\lambda x-\omega t)\}]
\end{aligned} \tag{29}$$

which show that the solution is periodic in x- and t-directions and that the amplitude functions vary only in the y-direction. $\hat{u}$ and $\hat{p}$ are the complex amplitude functions for velocities and pressure, respectively, the superscript asterisk denotes the complex conjugate. Substituting (29) in (23)–(28) and using (22), the following linearized equations are obtained for the amplitude functions:

$$(\mathrm{i}\lambda)\hat{u}_{\mathrm{f}}(y)+\frac{\partial\hat{v}_{\mathrm{f}}}{\partial y}=0 \tag{30}$$

$$\begin{aligned}
(1-C)Re[-\mathrm{i}\omega\hat{u}_{\mathrm{f}}(y)+\mathrm{i}\lambda(1-y^2)\hat{u}_{\mathrm{f}}(y)-2y\hat{v}_{\mathrm{f}}(y)] &= -(1-C)Re(\mathrm{i}\lambda)\hat{p}(y)+(\mathrm{i}\lambda)^2\hat{u}_{\mathrm{f}}\\
&\quad+\frac{\partial^2\hat{u}_{\mathrm{f}}}{\partial y^2}+CM(\hat{u}_{\mathrm{p}}-\hat{u}_{\mathrm{f}})
\end{aligned} \tag{31}$$

$$\begin{aligned}
(1-C)Re[-\mathrm{i}\omega\hat{v}_{\mathrm{f}}(y)+\mathrm{i}\lambda(1-y^2)\hat{v}_{\mathrm{f}}(y)] &= -(1-C)Re\frac{\partial\hat{p}}{\partial y}+(\mathrm{i}\lambda)^2\hat{v}_{\mathrm{f}}\\
&\quad+\frac{\partial^2\hat{v}_{\mathrm{f}}}{\partial y^2}+CM(\hat{v}_{\mathrm{p}}-\hat{v}_{\mathrm{f}})
\end{aligned} \tag{32}$$

$$(\mathrm{i}\lambda)\hat{u}_{\mathrm{p}}(y)+\frac{\partial\hat{v}_{\mathrm{p}}}{\partial y}=0 \tag{33}$$

$$\begin{aligned}
C\,Re\left[-\mathrm{i}\omega\hat{u}_{\mathrm{p}}(y)+\mathrm{i}\lambda\left(1-y^2+\frac{2}{M}\right)\hat{u}_{\mathrm{p}}(y)-2y\hat{v}_{\mathrm{p}}(y)\right] &= -C\,Re\frac{\rho_{\mathrm{f}}}{\rho_{\mathrm{p}}}(\mathrm{i}\lambda)\hat{p}(y)\\
&\quad+C\frac{\rho_{\mathrm{f}}}{\rho_{\mathrm{p}}}M(\hat{u}_{\mathrm{f}}-\hat{u}_{\mathrm{p}})
\end{aligned} \tag{34}$$

$$\begin{aligned}
C\,Re\left[-\mathrm{i}\omega\hat{v}_{\mathrm{p}}(y)+\mathrm{i}\lambda\left(1-y^2+\frac{2}{M}\right)\hat{v}_{\mathrm{p}}(y)\right] &= -C\,Re\frac{\rho_{\mathrm{f}}}{\rho_{\mathrm{p}}}\frac{\partial\hat{p}}{\partial y}\\
&\quad+C\frac{\rho_{\mathrm{f}}}{\rho_{\mathrm{p}}}M(\hat{v}_{\mathrm{f}}-\hat{v}_{\mathrm{p}})
\end{aligned} \tag{35}$$

Transferring the boundary conditions in (17) to the mean position of the wall, using the standard methods [42], the boundary conditions for the amplitude functions can be

obtained as

$$\begin{aligned}\tilde{u}_{\mathrm{f}}(\pm 1) &= -2 \text{ (Real part of } [\exp \mathrm{i}(\lambda x - \omega t)]) \\ \tilde{v}_{\mathrm{f}}(\pm 1) &= \text{Real part of } [\pm \mathrm{i}\omega \exp \mathrm{i}(\lambda x - \omega t)] \\ \tilde{v}_{\mathrm{p}}(\pm 1) &= 0\end{aligned} \tag{36}$$

The application of the boundary conditions at the mean surface has been considered appropriate so far as the amplitude of the wall is considered to be small and the wavelength is large.

The linearized boundary conditions are given by

$$\tilde{u}_{\mathrm{f}}(\pm 1) = -2, \quad \tilde{v}_{\mathrm{f}}(\pm 1) = \pm \mathrm{i}w, \quad \tilde{v}_{\mathrm{p}}(\pm 1) = \pm \mathrm{i}w \tag{37}$$

For rigid wavy wall, ω is zero and hence

$$\tilde{v}_{\mathrm{f}}(\pm 1) = 0, \quad \tilde{v}_{\mathrm{p}}(\pm 1) = 0 \tag{38}$$

The determination of the numerical solution of the particulate suspension flow through the wavy channel reduces to solving Equations (30)–(35) satisfying the boundary conditions (37). The numerical solution has been obtained by shooting technique and the results are presented in the next section. It may be pointed out that except for the linearization of the governing equations of the particulate suspension flow, no other approximation has been used in the derivation.

3. NUMERICAL SOLUTION

To solve numerically, the linearized equations (30)–(35) along with the inhomogeneous boundary conditions (37), the equations are expressed as a system of six first-order ordinary differential equations. Defining the variables z_j, $j = 1, 2, \ldots, 6$ as

$$z_1 = \hat{u}_{\mathrm{f}}, \quad z_2 = \dot{\hat{u}}_{\mathrm{f}}, \quad z_3 = \hat{v}_{\mathrm{f}}, \quad z_4 = \hat{p}, \quad z_5 = \hat{u}_{\mathrm{p}}, \quad z_6 = \hat{v}_{\mathrm{p}} \tag{39}$$

where the dot above the variable represents differentiation with respect to y, Equations (30)–(35) can be written as

$$\begin{aligned}\dot{z}_1 &= z_2 \\ \dot{z}_2 &= (1-C)Re[-\mathrm{i}\omega z_1 + \mathrm{i}\lambda(1-y^2)z_1 - 2yz_3] + (1-C)Re\ \mathrm{i}\lambda z_4 - (\mathrm{i}\lambda)^2 z_1 - CM(z_5 - z_1) \\ \dot{z}_3 &= -\mathrm{i}\lambda z_1 \\ \dot{z}_4 &= \frac{1}{(1-C)Re}[(\mathrm{i}\lambda)^2 z_3 - (\mathrm{i}\lambda)z_2 + CM(z_6 - z_3)] + \mathrm{i}\omega z_3 - (\mathrm{i}\lambda)(1-y^2)z_3 \\ \dot{z}_5 &= \frac{(\rho_{\mathrm{f}}/\rho_{\mathrm{p}})M[z_2 - (\mathrm{i}\lambda)(z_3 - z_6)] - Re[-2z_6 - \lambda\omega z_6 - (\mathrm{i}\lambda)^2(1 - y^2 + 2/M)z_6]}{Re[-\mathrm{i}\omega + \mathrm{i}\lambda(1 - y^2 + 2/M)] + (\rho_{\mathrm{f}}/\rho_{\mathrm{p}})M} \\ \dot{z}_6 &= -\mathrm{i}\lambda z_5\end{aligned} \tag{40}$$

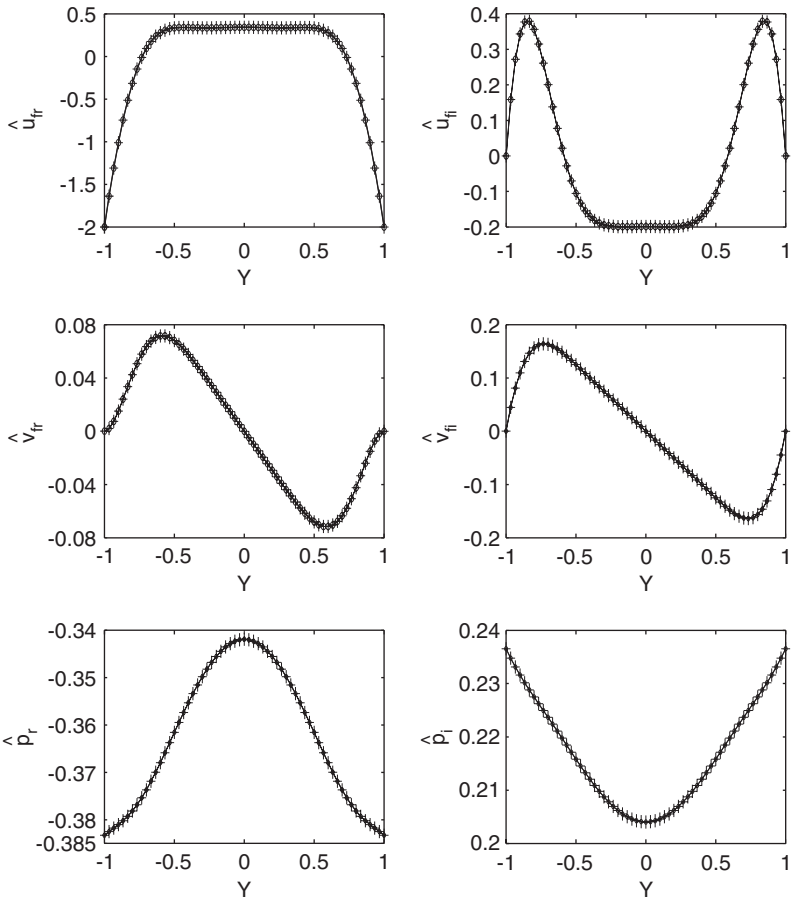

Figure 2. Comparison of amplitude function of the perturbed quantities for the wavy channel flow $Re = 150$, $\lambda = 0.738$, $\varepsilon = 0.1$: –○–, Selvarajan [43]; –|–, present method applied to Newtonian model.

Equation (40) with boundary conditions (37) have been solved by shooting technique. The results obtained for the case of viscous incompressible fluid by the present method are compared (Figure 2) with those presented by Selvarajan [43] for Newtonian flow through wavy channels. They employ finite difference method of Scott and Watts [44] and spectral collocation method of Canuto *et al.* [45]. The close agreement gives the confidence in the applicability of the method in the determination of the particulate suspension flow through wavy-walled channels.

3.1. Computational results for particulate suspension flow through rigid wavy channel

The flow through rigid wavy channel described by the system of ordinary differential equations (40) subject to the boundary conditions (37) with $\omega = 0$ has been solved by

shooting technique using MATLAB subroutine which solves two-point boundary-value problems (BVPS) for ordinary differential equations by collocation method. It integrates a system of ordinary differential equations of the form $y' = f(x, y)$ on the interval $[a, b]$, subject to general two-point boundary conditions and produces a solution that is continuous on $[a, b]$ and has a continuous first derivative there. The resulting equations are solved by starting with parameter values for which one can get a solution, and use it as a guess for the remaining iterations. The processes are repeated until the solution converges. The values of parameters have been taken as density ratio $(\rho_p/\rho_f) = 2$ and ratio of particle radius to half the width of the channel $(a/d) = 0.02$, with the grid size of 281×101. Following guidelines from Selvarajan [43], trials were made with $51, 101, 181$ and 281 grid lines along x-axis and $21, 41, 61, 81$ and 101 grid lines along y-axis. The results are found to be grid independent for 281×101 size. Further refinement of the grid did not produce significant changes in the result and therefore the results have been obtained with the above grid.

Computations are performed for the parameters of the rigid wavy-walled channel flow with $Re = 150, \lambda = 1$ and $\omega = 0$ for two values of the volume fraction density C of the particles (0 and 0.5). The values of Re and λ correspond to those of Selvarajan [43]. The amplitude functions for the flow in a wavy channel describing the fluid and particulate phase velocities $\hat{u}_f, \hat{v}_f, \hat{u}_p$, and $\hat{v}_p (\hat{u}_f = \hat{u}_{fr} + i\hat{u}_{fi}; \hat{v}_f = \hat{v}_{fr} + i\hat{v}_{fi}; \hat{u}_p = \hat{u}_{pr} + i\hat{u}_{pi}; \hat{v}_p = \hat{v}_{pr} + i\hat{v}_{pi})$ are plotted in Figure 3. It may be pointed out that the results presented for $C = 0$ by the present numerical method agree with those predicted by Selvarajan [43], correct to four decimal place accuracy. It is seen that for the case with $C = 0.5$, the peaks of $\hat{u}_{fr}, \hat{v}_{fr}, \hat{u}_{fi}$, and $\hat{v}_{fi}$ are generally slightly lower than those for $C = 0$. The distributions of $\hat{u}_{pr}, \hat{v}_{pr}, \hat{u}_{pi}$, and $\hat{v}_{pi}$ with y are same as those for $\hat{u}_{fr}, \hat{v}_{fr}, \hat{u}_{fi}$, and $\hat{v}_{fi}$, respectively. This is a consequence of the assumption of uniform volume fraction density of small particles. Figure 4 shows the variation of perturbed velocities for $C = 0.5$. Since variations of $\hat{u}_{fr}, \hat{v}_{fr}$ and others are similar for $C = 0$ and 0.5, the plots of $\tilde{u}_f, \tilde{v}_f$ for $C = 0$ are not shown. From the results of the amplitude functions, the various flow quantities have been computed and presented in Figures 5–7. It is observed (Figure 5) that (a) the maximum values of $\tilde{p}$ lies slightly downstream of the maximum channel cross-section and (b) the amplitude of $\tilde{p}$ increases with increase in volume fraction density, the effect of $C = 0.5$ changes maximum of $\tilde{p}$ from 0.4 to 0.5 (Figure 5(c) and (d)). Figure 6 shows the variation of velocities in a rigid wavy channel for $C = 0.5$. Figure 7 shows the variation of $\tilde{\tau}$ in a rigid wavy channel. It is observed that the maximum value of $\tilde{\tau}$ increases with increase in volume fraction density. This is because of the increase in suspension viscosity with increase in volume fraction density.

3.1.1. Effect of Re and ε. The magnitude of wall shear stress, τ_w, is important in many applications. The effects of the Reynolds number, Re, amplitude parameter, ε, volume fraction density, C, of the particles on the wall shear stress have been examined. Figure 8 presents τ_w for rigid channel $(\omega = 0)$ with $\varepsilon = 0.1$ and $\lambda = 1.0$ for various values of Re and C. Results for $\varepsilon = 0.2$ and 0.3 show similar trends. It is observed that (i) for $C = 0$, the peak value of τ_w occurs very slightly upstream of the maximum channel cross-section. With increase in Reynolds number, the peak shifts towards upstream and the profiles at higher Reynolds number display increasing asymmetry. The profiles for Reynolds number greater than 50 show a negative peak towards the end of the channel. The magnitude of the peak increases with Re. These results are same as those of Selvarajan *et al.* [8] and (ii) for $C = 0.3$, the profiles are similar to those of $C = 0$. However, the magnitudes of the peak values are higher on the

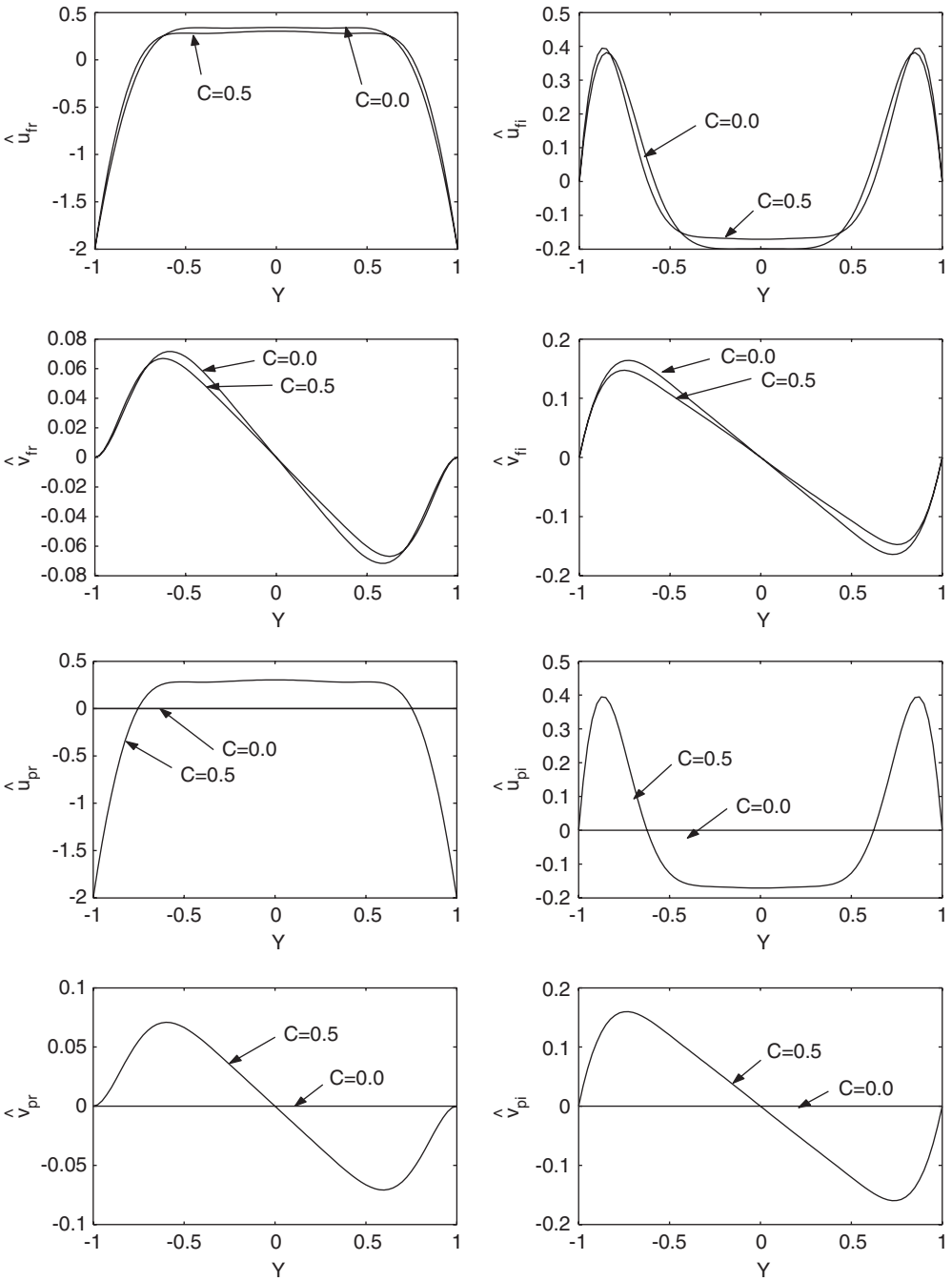

Figure 3. Amplitude function of the perturbed velocities for the wavy channel flow for two volume fraction densities, $Re = 150,\ \lambda = 1,\ \varepsilon = 0.1$.

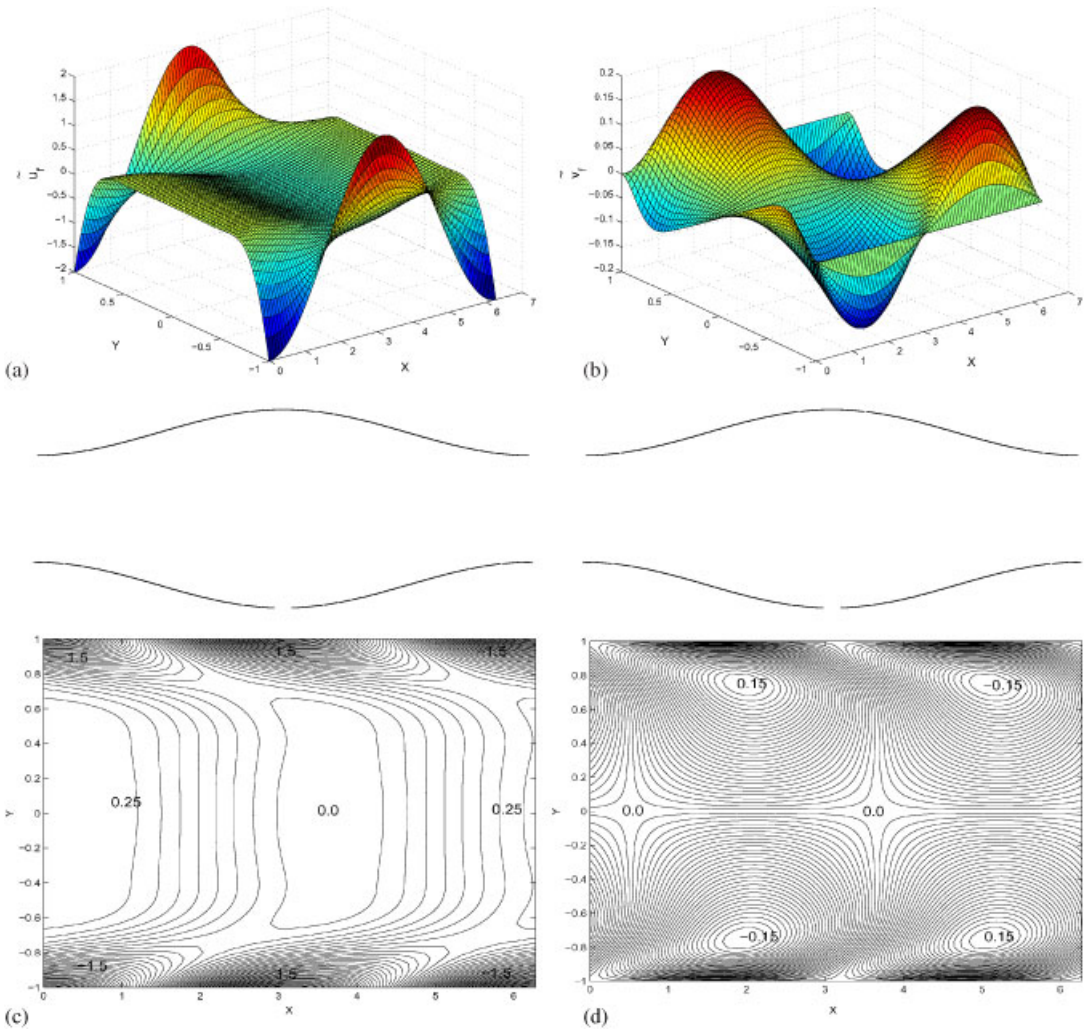

Figure 4. Variation of perturbed velocities for rigid wavy channel flow: $Re = 150$, $\lambda = 1.0$, $\varepsilon = 0.1$, $\omega = 0$, $C = 0.5$: (a) mesh plot of $\tilde{u}_f$; (b) mesh plot of $\tilde{v}_f$; (c) contour plot of $\tilde{u}_f$; and (d) contour plot of $\tilde{v}_f$.

positive and on the negative sides. The profile shows the negative peak even at $Re = 50$ and (iii) for $C = 0.5$, the positive and negative peaks are increased further. With increase in ε, the peak values of wall shear stress increase.

In the case of two-dimensional flow through a rigid channel, the separation and reattachment points are the locations where the shear stress on the wall is zero. Further, the value of Reynolds number for which the flow just separates is called the critical Reynolds number, Re_{cr}. For $\varepsilon = 0.1$, the shear-stress variation is negative and the flow is attached for Reynolds number below 600 when $C = 0$, whereas for $C = 0.3$ and 0.5, the flow is attached only

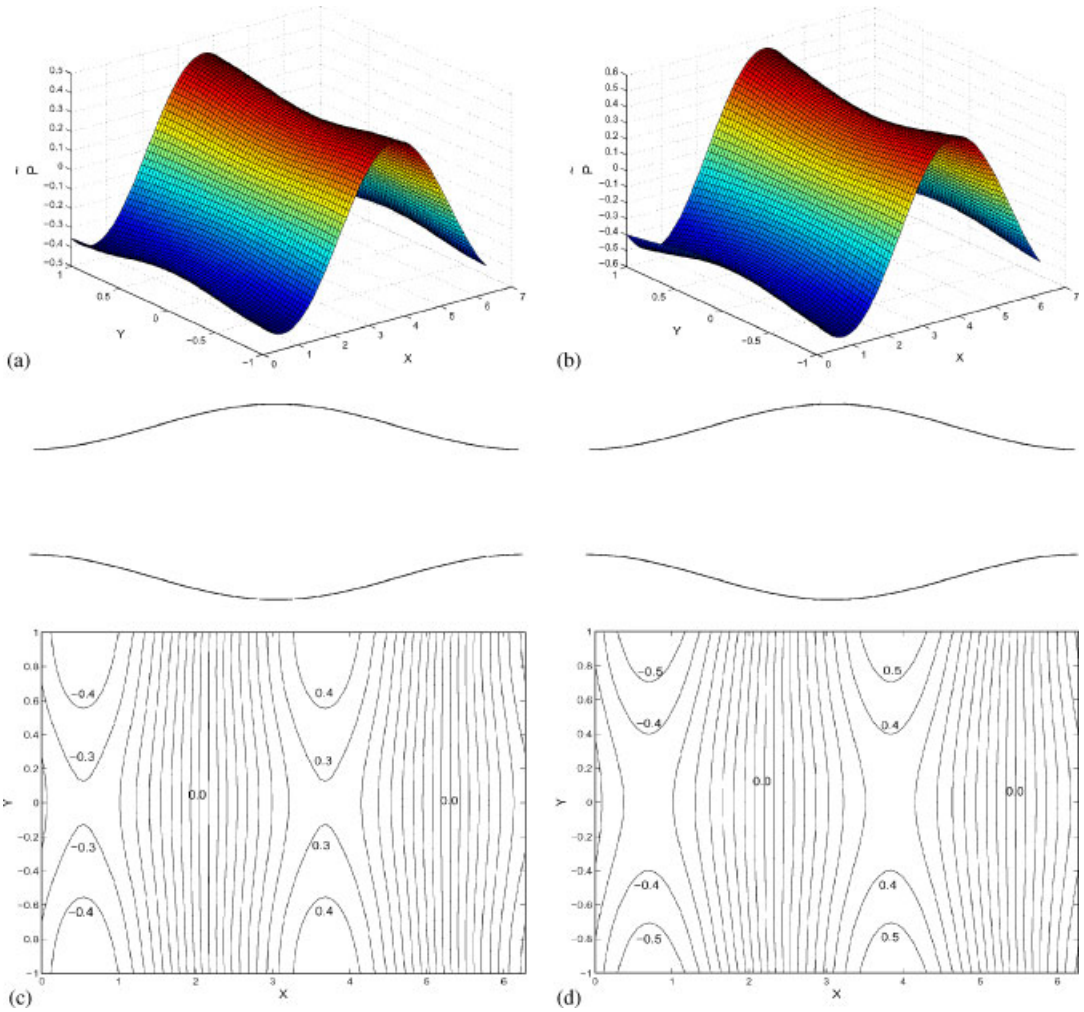

Figure 5. Variation of perturbed pressure, $\tilde{p}$ for the flow in a rigid wavy channel: $Re = 150$, $\lambda = 1.0$, $\omega = 0$, $\varepsilon = 0.1$: (a) mesh plot of $\tilde{p}$ for $C = 0.0$; (b) mesh plot of $\tilde{p}$ for $C = 0.5$; (c) contour plot of $\tilde{p}$ for $C = 0.0$; and (d) contour plot of $\tilde{p}$ for $C = 0.5$.

below $Re = 425$ and 350, respectively (Figure 8). It is observed that (i) for $\varepsilon = 0.2$, the flow is attached only when Re is less than 50 for $C = 0$. On the other hand, for $C = 0.3$ and 0.5, Re_{cr} is equal to 38 and 30, respectively and (ii) for $\varepsilon = 0.3$, $Re_{cr} = 10$, 5 and 3 for $C = 0$, 0.3 and 0.5, respectively. Figure 9 shows the positions of separation and reattachment points for $\varepsilon = 0.1, 0.2$ and 0.3 when $C = 0.0, 0.3, 0.5$. Figure 10 shows the variation of the Re_{cr} with ε and C. It is observed that with the increase of ε, the critical Reynolds number decreases for a fixed value of C. With the increase of volume fraction density of the particles, a further decrease in the critical Reynolds number is seen.

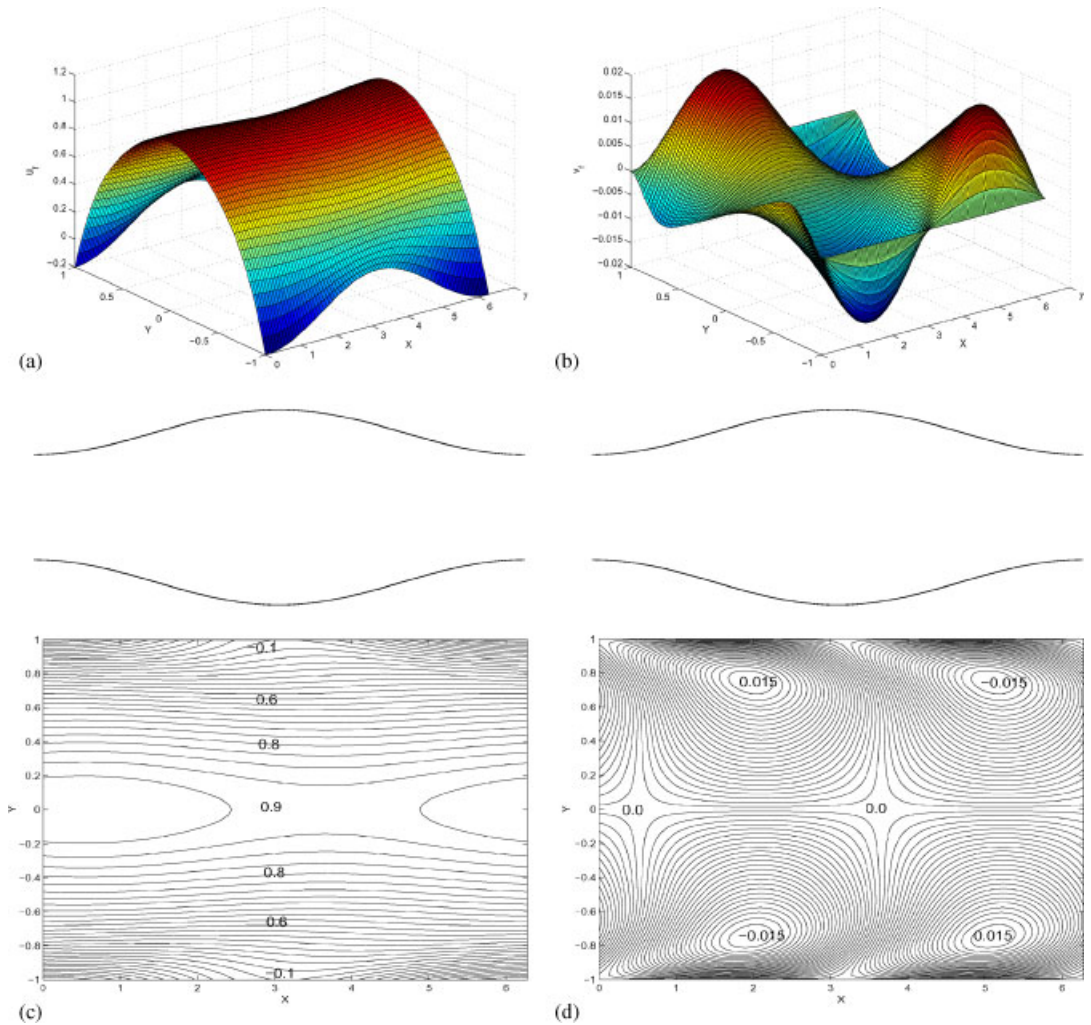

Figure 6. Variation of velocities for the flow in a rigid wavy channel: $Re = 150$, $\lambda = 1.0$, $\varepsilon = 0.1$, $\omega = 0$, $C = 0.5$: (a) mesh plot of u_f; (b) mesh plot of v_f; (c) contour plot of u_f; and (d) contour plot of v_f.

3.2. Numerical solution for wave-excited channel flow of particulate suspension

3.2.1. Development of asymmetry at low Reynolds numbers. In their study on peristaltic motion of Newtonian viscous fluid at low Reynolds numbers, Burns and Parkes [1] observed that the velocity profiles are symmetric about x-axis at all cross-sections. However, Selvarajan *et al.* [8] have been able to show the development of asymmetry at $Re = 0.6$. They have observed that the flow field gains symmetry as Re approaches the value of 0.001 and their results agree well with those of Burns and Parkes [1] for this Re. They attributed the failure of Burns and Parkes [1] model in not observing asymmetry to the neglect of inertia effects in their study. However, the formulation by Selvarajan *et al.* [8] has permitted the numerical solution

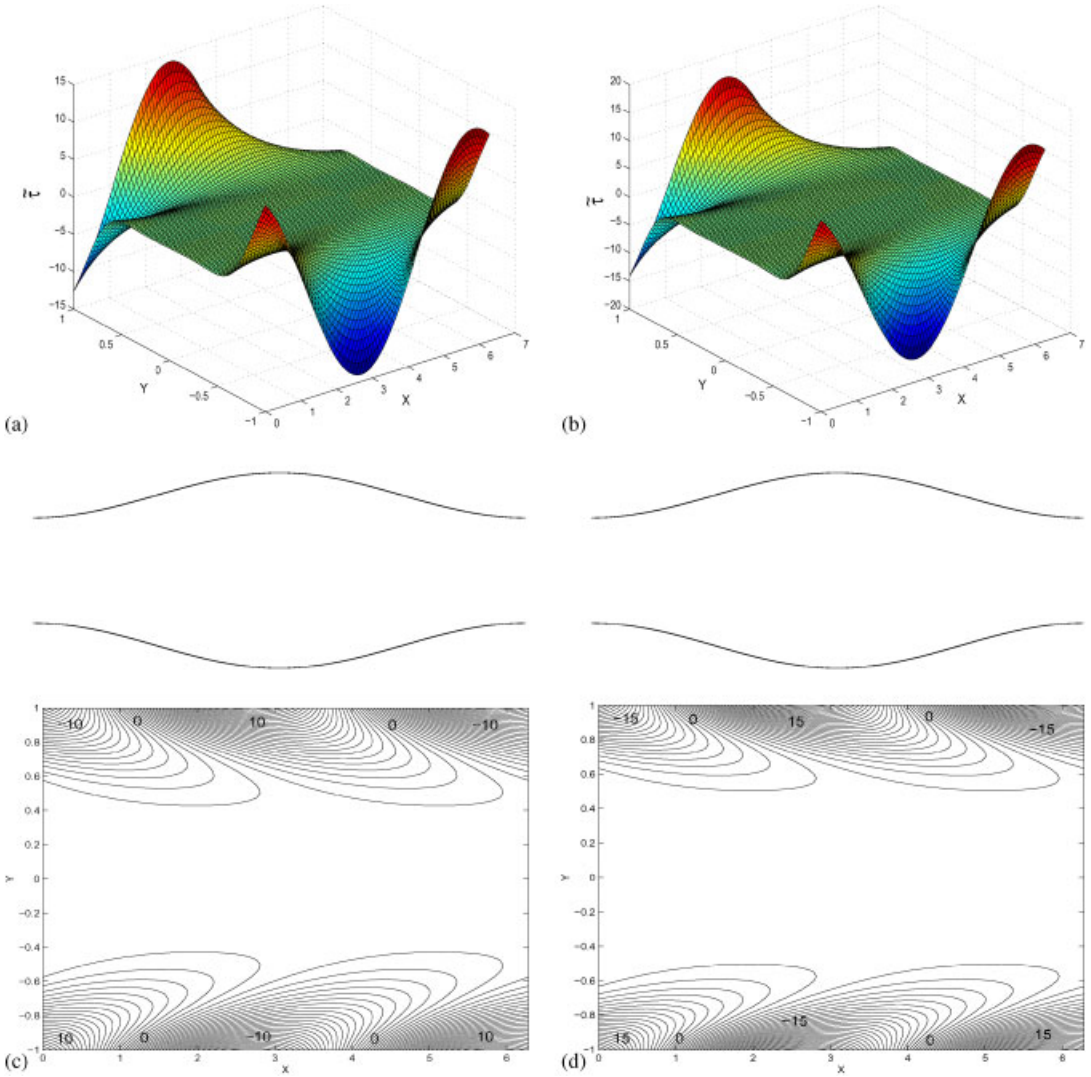

Figure 7. Variation of shear stress, $\tilde{\tau}$ for the flow in a rigid wavy channel: $Re = 150$, $\lambda = 1.0$, $\varepsilon = 0.1$, $\omega = 0$: (a) mesh plot of $\tilde{\tau}$ for $C = 0$; (b) mesh plot of $\tilde{\tau}$ for $C = 0.5$; (c) contour plot of $\tilde{\tau}$ for $C = 0$; and (d) contour plot of $\tilde{\tau}$ for $C = 0.5$.

for peristaltic motion in the limit $Re \to 0$ while retaining the inertia terms. To examine this for flow with particulate suspension, computations with $\varepsilon = 0.1$, $\lambda = 0.25$, $\omega = 4\pi$, $C = 0.0$ and 0.3 were carried out at $Re = 0.025$, 0.15 and 0.6. Table I shows the variations of centreline velocity, u_f along x-axis. The computated results for $Re = 0.6$ and 0.15 reveal the development of asymmetry in the channel for both $C = 0$ and 0.3. It is interesting to note that at low Re of 0.025 values of u_f show symmetry and are almost identical for $C = 0$ and 0.3.

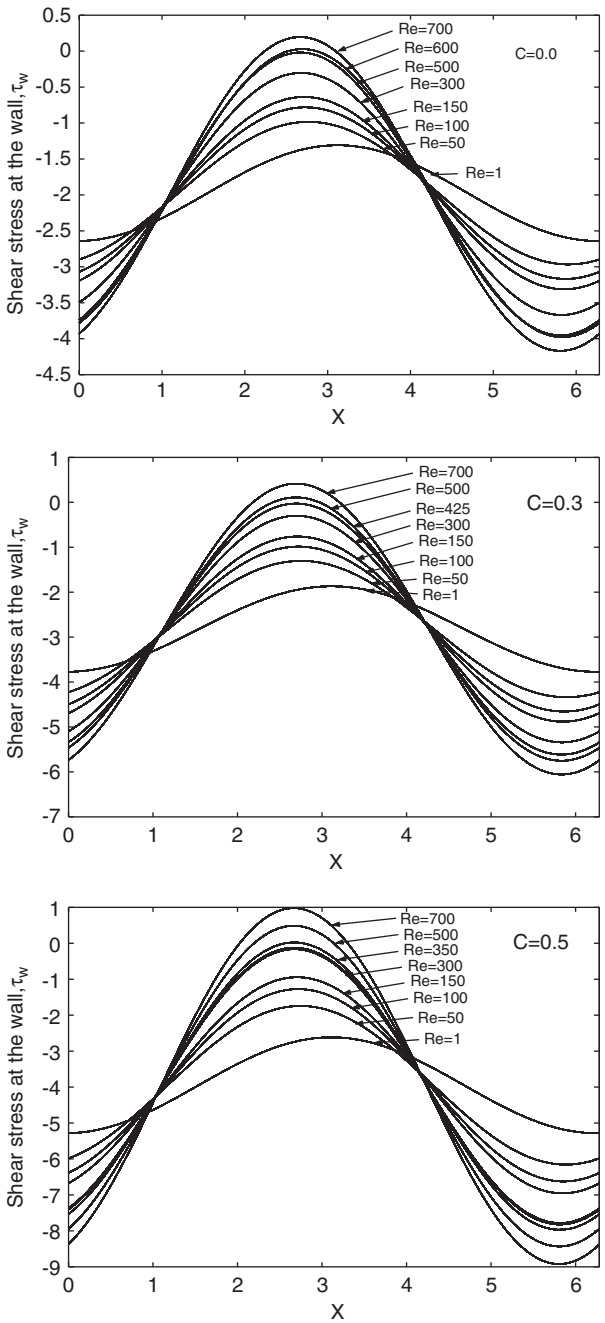

Figure 8. Variation of shear stress at the wall for the wavy channel flow for different Reynolds numbers when $\varepsilon = 0.1, \lambda = 1.0$, and $\omega = 0$.

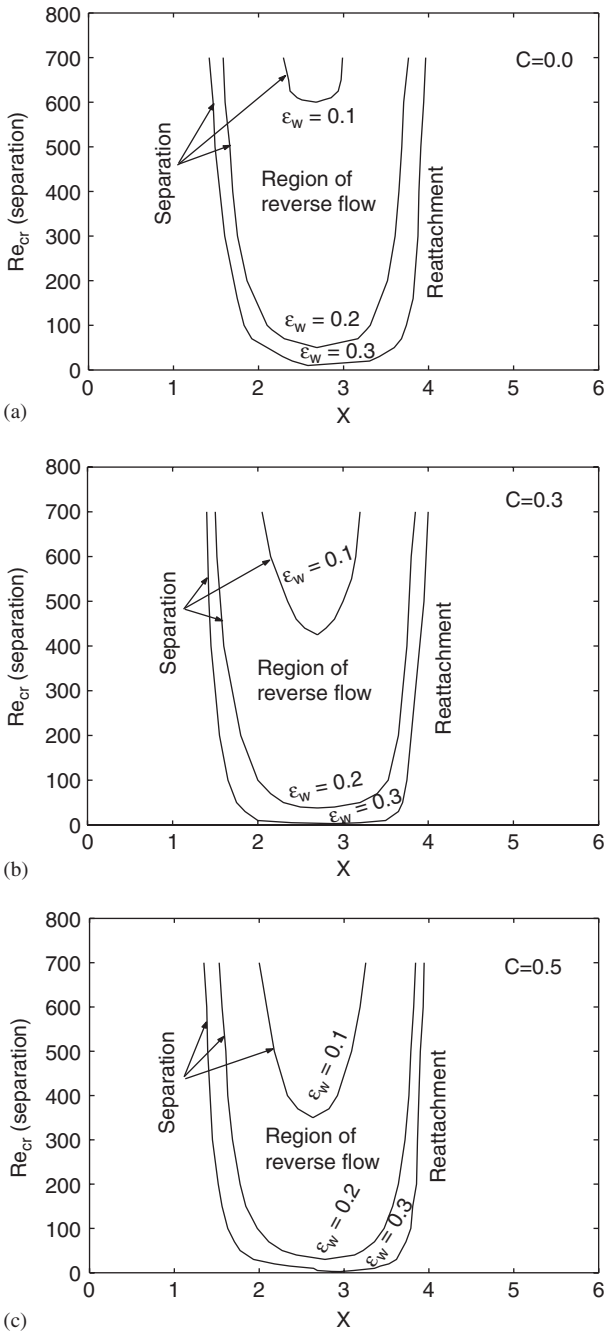

Figure 9. Location of separation and reattachment points for the wavy channel flow with Reynolds numbers when $\lambda = 1.0$: (a) $C = 0.0$; (b) $C = 0.3$; and (c) $C = 0.5$.

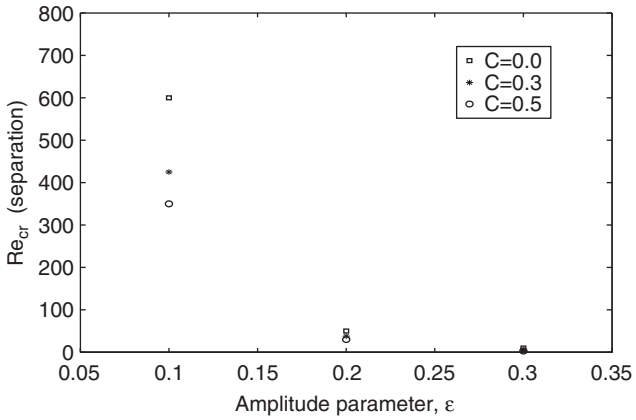

Figure 10. Variation of critical Reynolds number for separation with wall amplitude for different values of volume fraction density in the wavy channel flow, $\lambda = 1.0$.

Table I. Variation in centreline velocity u_f of the fluid phase with Reynolds number for different volume fraction densities, $\varepsilon = 0.1$, $\lambda = 0.25$ and $\omega = 4\pi$.

	$Re = 0.6$		$Re = 0.15$		$Re = 0.025$	
x(rad)	$c = 0.0$	$c = 0.3$	$c = 0.0$	$c = 0.3$	$c = 0.0$	$c = 0.3$
0	−0.1215	−0.1180	−0.1273	−0.1275	−0.1278	−0.1277
0.7854	−0.0687	−0.0641	−0.0810	−0.0815	−0.0840	−0.0838
1.5708	0.0360	0.0389	0.0245	0.0238	0.0207	0.0209
2.3562	0.1312	0.1309	0.1272	0.1269	0.1249	0.1250
3.1416	0.1613	0.1578	0.1671	0.1673	0.1676	0.1676
3.9270	0.1085	0.1039	0.1288	0.1213	0.1238	0.1236
4.7124	0.0038	0.0009	0.0153	0.0159	0.0191	0.0189
5.4974	−0.0915	−0.0911	−0.0874	−0.0871	−0.0851	−0.0852
6.2832	−0.1215	−0.1180	−0.1273	−0.1275	−0.1278	−0.1277

Comparison of the contour plots (not shown) of fluid velocity, particle velocity and pressure contours at $Re = 0.025$ and 0.6 show the distortions due to asymmetry at $Re = 0.6$ as observed by Selvarajan *et al.* [8].

3.2.2. Variations in flow variables with frequency. In order to show the effects of frequency ω and C in a wave-excited channel, the amplitude functions of perturbed velocities and the maximum shear stress and pressure at the wall are computed for different values of C and ω. Figure 11 presents the effect of ω. It is seen that with increase in ω, for fixed values of Re and C, the amplitude functions of perturbed velocities decrease. The values of parameters are chosen to facilitate comparison of the present results with those of Selvarajan *et al.* [8] for the Newtonian model. Figure 12 presents the amplitude functions of the perturbed velocities for both the fluid and particulate phases for different values of C, namely, 0, 0.3 and 0.5, with $Re = 150$, $\varepsilon = 0.1$, $\lambda = 1.058$, $\omega = 0.4$. It is observed that the variations in the peaks of

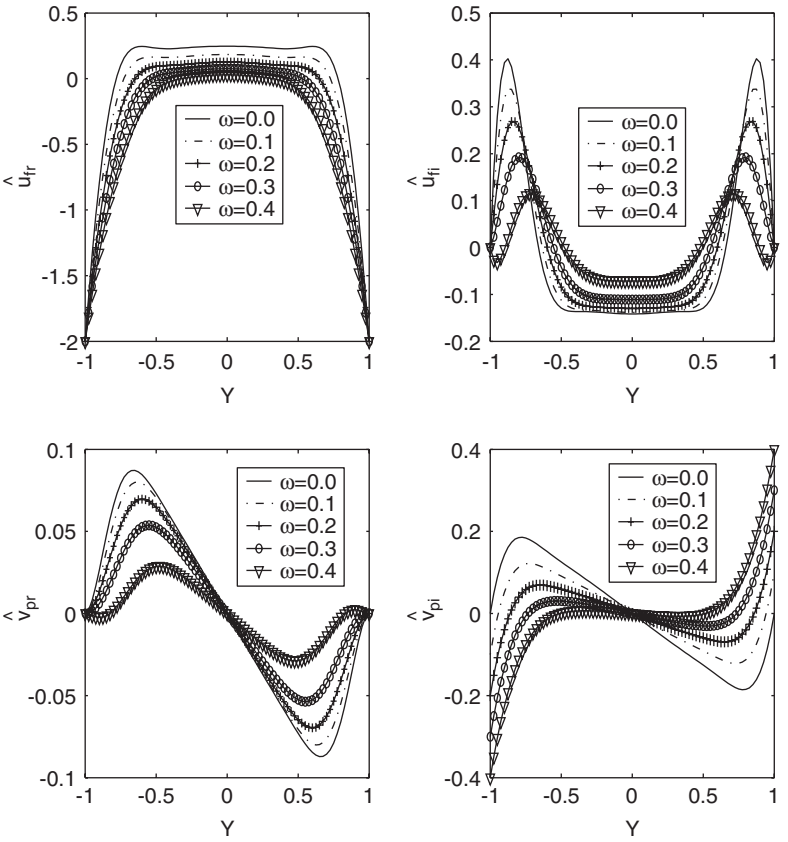

Figure 11. Amplitude function of the perturbed velocities for the wave-excited channel flow for different frequencies of wave excitation, $Re = 150, \varepsilon = 0.1, \lambda = 1.058$ and $C = 0.5$.

$\hat{u}_{\mathrm{fr}}, \hat{u}_{\mathrm{pr}}, \hat{v}_{fi}$, and $\hat{v}_{\mathrm{pi}}$ are very small, whereas the peaks of $\hat{v}_{\mathrm{fr}}, \hat{v}_{\mathrm{pr}}, \hat{u}_{\mathrm{fi}}$, and $\hat{u}_{\mathrm{pi}}$ decrease as C increases. Figure 13 shows the variations of pressure perturbation and shear stress at the wall with the frequency ω and the wave number λ for $C = 0.0, 0.3$ and 0.5, with $Re = 1000$. It is observed that (i) for $C = 0$, the $\tau_{\mathrm{w(max)}}$ has a minimum at $\omega = 0.2$, whereas when $C = 0.3$ and 0.5, the minimum $\tau_{\mathrm{w(max)}}$ occurs at $\omega = 0.3$. Subsequently, the value of $\tau_{\mathrm{w(max)}}$ increases with increase in ω in all cases (Figure 13(a)) and (ii) with increase in ω, the $\tilde{p}_{\mathrm{w(max)}}$ remains nearly constant for $C = 0$ and 0.3, whereas for $C = 0.5$, it increases linearly (Figure 13(b)). To examine this increase in $\tilde{p}_{\mathrm{w(max)}}$, computations were repeated for C between 0.2 and 0.5 at smaller intervals which reveal the rapid increase between $C = 0.3$ and 0.5 (Figure 14) and (iii) for $C = 0$, the $\tau_{\mathrm{w(max)}}$ has a minimum at $\lambda = 0.3$, whereas for $C = 0.3$ and 0.5, the $\tau_{\mathrm{w(max)}}$ is minimum at $\lambda = 0.2$. Subsequently, it increases till $\lambda = 0.6$ and then decreases again (Figure 13(c)) and (iv) the $\tilde{p}_{\mathrm{w(max)}}$ increases with increase in C for fixed values of λ and ω and has maximum value when $\lambda = 0.2$. It decreases after $\lambda = 0.2$ and remains constant for a fixed value of C (Figure 13(d)).

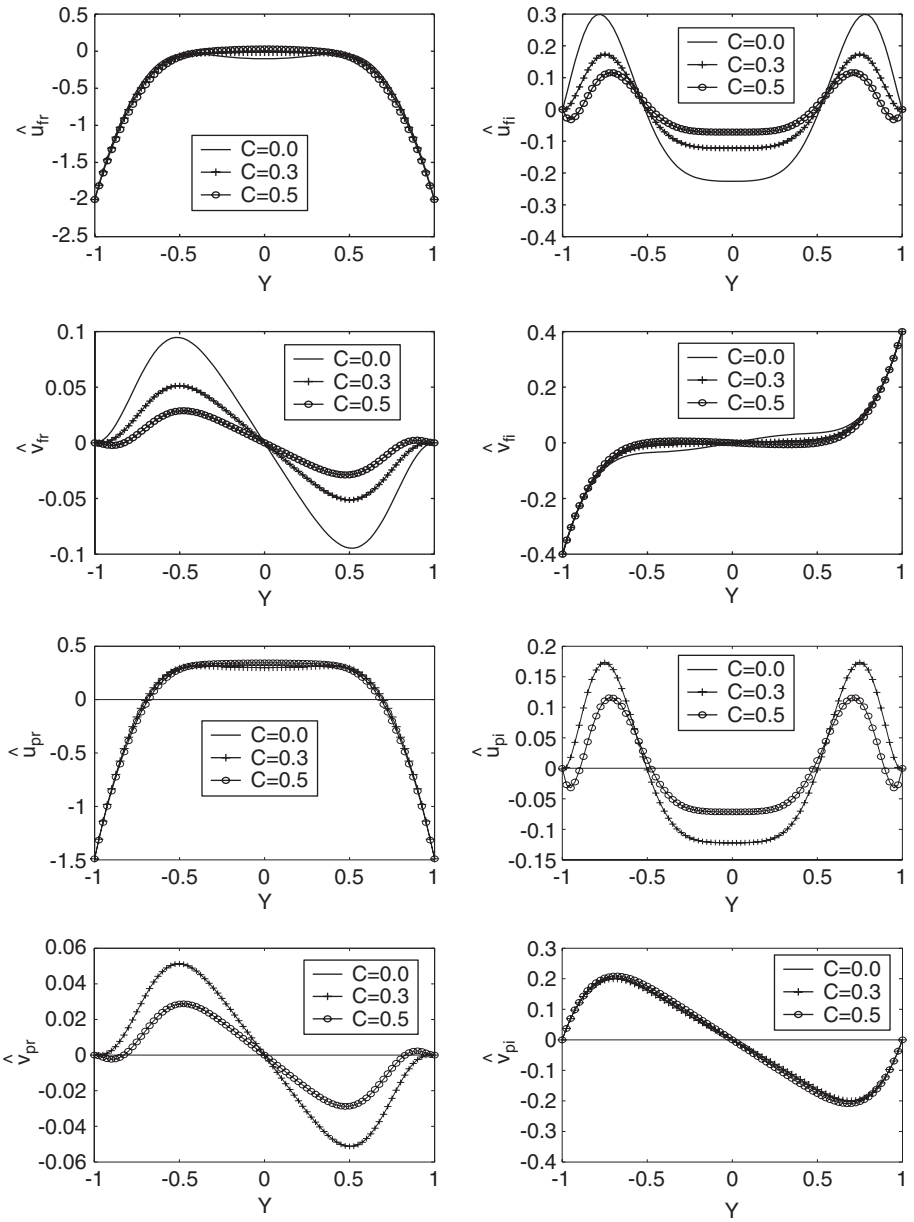

Figure 12. Amplitude function of the perturbed velocities for the wave-excited channel flow for different volume fraction densities, $Re = 150$, $\lambda = 1.058$, $\omega = 0.4$ and $\varepsilon = 0.1$.

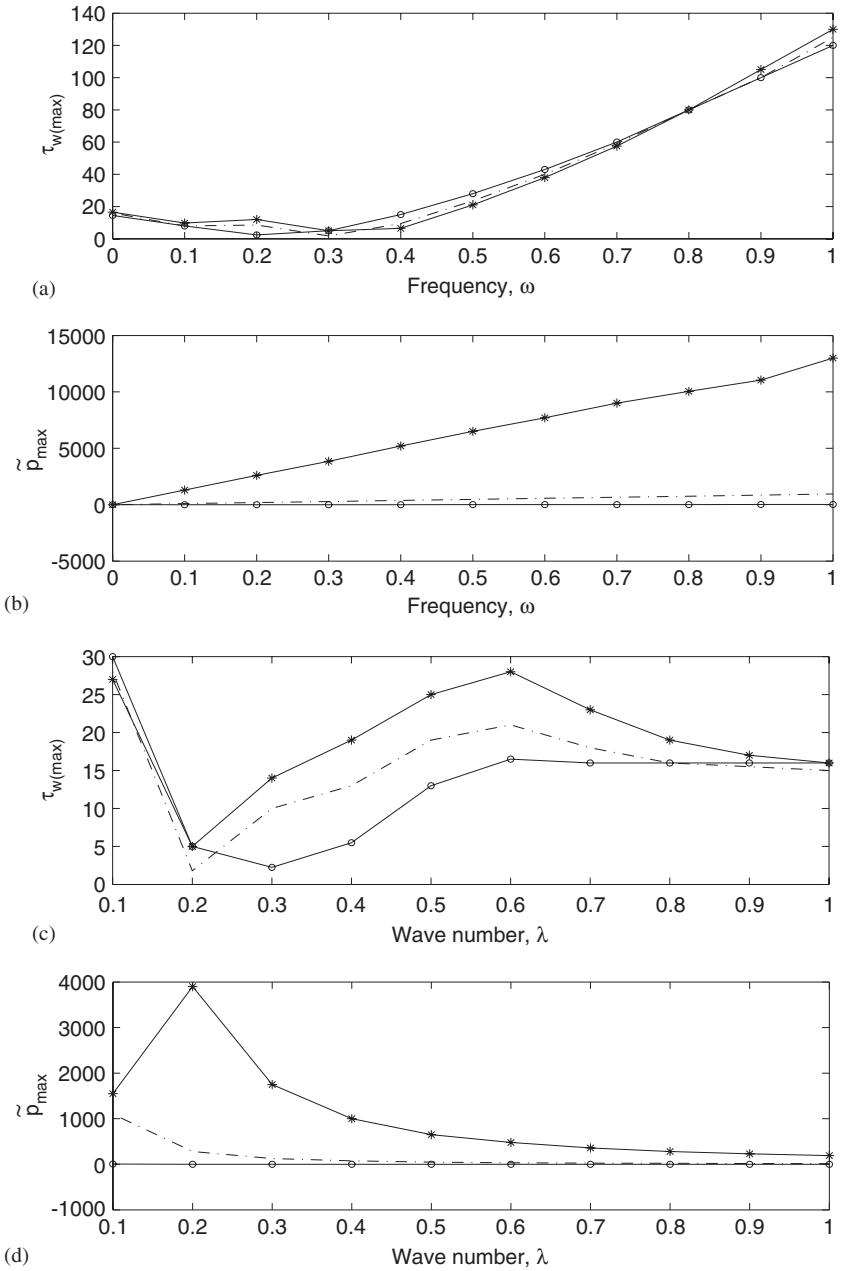

Figure 13. Variation of maximum shear stress and pressure perturbation at the wall for wave-excited channel flow for different volume fraction densities: –○–, $C = 0.0$; ·—·, $C = 0.3$; –★–, $C = 0.5$. (a), (b) with ω as parameter, $Re = 1000$, $\lambda = 0.2$, $\varepsilon = 0.2$ and (c), (d) with λ as parameter, $Re = 1000$, $\omega = 0.3$ and $\varepsilon = 0.2$.

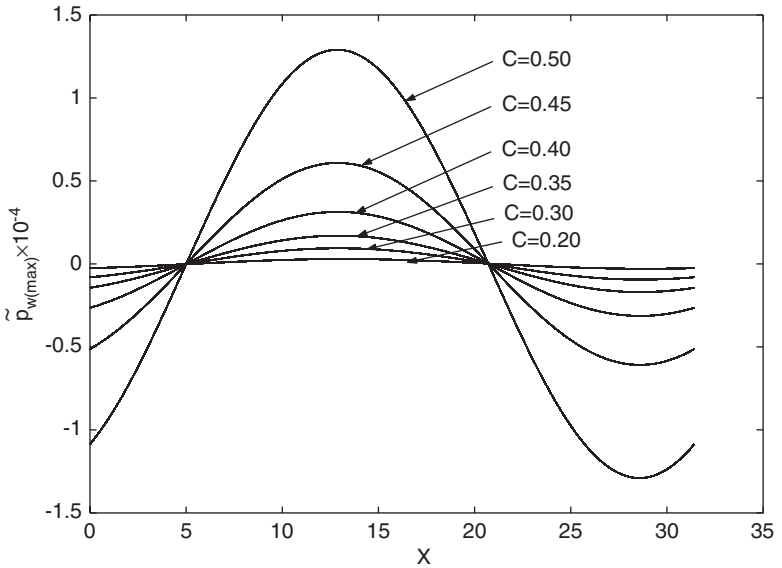

Figure 14. Variation of maximum pressure perturbation at the wall for wave-excited channel flow for different volume fraction densities when $Re = 1000, \varepsilon = 0.2, \lambda = 0.2$ and $\omega = 1$.

4. CONCLUSION

Continuum equations governing the two-phase particulate suspension flow are developed and the flow of particulate suspension in wave-excited channel is investigated using a combination of a perturbation approach and numerical simulation. The mathematical model considered in the present study incorporate the effects of finite particulate volume fraction. The constant volume fraction assumption employed in the study allows the governing equations for the base flow to be solved analytically. The solutions for the wave-excited channel flow are obtained as a perturbation from the parabolic velocity profile of the fully developed particulate suspension flow in a straight channel. The computational results obtained for the flow in a rigid wavy channel agree with the available results for the Newtonian flows.

For rigid wavy channel, the change of volume fraction density does not significantly affect the fluid and particulate velocities. However, the pressure perturbation and wall shear stress are affected significantly. The amplitude of pressure perturbation increases with increase in volume fraction density.

With regard to the wall shear stress (τ_w), the following is observed. For $C = 0$, τ_w is negative for low values of Re. As Re increases, the negative peak in the trough region becomes more negative and less negative in the crest region. The Reynolds number at which the value in the crest region becomes zero is the critical Reynolds number (Re_{cr}). For the particulate suspension flow ($C > 0$), the values of τ_w at low Re are more negative than those $C = 0$. However as Re increases the increase in the crest value is more rapid, when $C > 0$. Hence the Re_{cr} is lowered as C increases. As waviness increases, the Re_{cr} decreases further.

For the flow through wave-excited channel, the amplitude functions of different velocities decrease with increase in ω. The amplitude functions decrease further with volume fraction density.

ACKNOWLEDGEMENTS

The computations are a part of project funded by Council of Scientific and Industrial Research, India. Computations have been carried out at the Department of science and technology funded centre for CFD. Support of funding agencies is gratefully acknowledged.

The authors sincerely thank the referee for his very useful comments and suggestions. The References [40, 41] suggested by him have helped us in understanding the boundary conditions on the rough wall. The authors also thank the Editor, Prof. Nigel P. Weatherill for his encouraging remarks.

REFERENCES

1. Burns JC, Parkes T. Peristaltic motion. *Journal of Fluid Mechanics* 1967; **29**:731–743.
2. Shapiro AH, Jaffrin MY, Weinberg SL. Peristaltic pumping with long wavelengths at low Reynolds numbers. *Journal of Fluid Mechanics* 1969; **37**:799–825.
3. Fung YC, Yih CS. Peristaltic transport. *Journal of Applied Mechanics* (ASME) 1968; **33**:669–675.
4. Chow TS. Peristaltic transport in a circular cylinder pipe. *Journal of Applied Mechanics—Transactions of the ASME* 1970; **37**:901–905.
5. Takabatake S, Ayukawa K. Numerical study of two-dimensional peristaltic flows. *Journal of Fluid Mechanics* 1982; **122**:439–465.
6. Takabatake S, Ayukawa K, Mori A. Peristaltic pumping in circular cylinder tubes: a numerical study of fluid transport and its efficiency. *Journal of Fluid Mechanics* 1988; **193**:269–283.
7. Misra JC, Pandey SK. Peristaltic transport in a tapered tube. *Mathematical and Computer Modelling* 1995; **22**:137–151.
8. Selvarajan S, Tulapurkara EG, Vasanta Ram V. A numerical study of flow through wavy walled channels. *International Journal for Numerical Methods in Fluids* 1998; **26**:519–531.
9. Selvarajan S, Tulapurkara EG, Vasanta Ram V. Stability characteristics of wavy walled channel flows. *Physics of Fluids* 1999; **11**:579–589.
10. Hung TK, Brown TD. Solid-particle motion in two dimensional peristaltic flows. *Journal of Fluid Mechanics* 1976; **73**:77–96.
11. Kaimal MR. Peristaltic pumping of a Newtonian fluid with particles suspended in it at low Reynolds number under long wavelength approximation. *Journal of Applied Mechanics—Transactions of the ASME* 1978; **45**:32–36.
12. Srivastava LM, Srivastava VP. Peristaltic transport of a particle-fluid suspension. *Journal of Biomechanical Engineering-Transactions of the ASME* 1989; **111**:157–165.
13. Misra JC, Pandey SK. Peristaltic transport of a particle-fluid suspension in a cylindrical tube. *Computers and Mathematics with Applications* 1994; **28**:131–145.
14. Marble FE. Dynamics of dusty gases. *Annual Review of Fluid Mechanics* 1970; **2**:397–446.
15. Ishii M. *Thermo-Fluid Dynamic Theory of Two-Phase Flow*. Eyrolles: Paris, 1975.
16. Soo SL. *Particulates and Continuum*: *Multiphase Fluid Dynamics*. Hemisphere: New York, 1989.
17. Berlemont A, Desjonqueres P, Gouesbet G. Particle Lagrangian simulation in turbulent flows. *International Journal of Multiphase Flow* 1990; **19**:19–34.
18. Berlemont A, Grancher MS, Gouesbet G. On the Lagrangian simulation of turbulence influence on droplet evaporation. *International Journal of Heat and Mass Transfer* 1991; **34**:2805–2812.
19. Di Giovanni PR, Lee SL. Impulsive motion in a particle-fluid suspension including particulate volume, density and migration effects. *Journal of Applied Mechanics* 1974; **41**:35–41.
20. Drew DA. Application of general constitutive principles to the derivation of multidimensional two-phase flow equations. *International Journal of Multiphase Flow* 1979; **5**:143–264.
21. Drew DA. Mathematical modeling of two-phase flow. *Annual Review of Fluid Mechanics* 1983; **15**:261–291.
22. Tam CKW. The drag on a cloud of spherical particles in low Reynolds number flow. *Journal of Fluid Mechanics* 1969; **38**:537–546.
23. Nayfeh AH. Oscillating two-phase flow through a rigid pipe. *AIAA Journal* 1966; **4**:1868–1871.
24. Chamkha AJ. Hydromagnetic two-phase flow in a channel. *International Journal of Engineering Science* 1995; **33**:437–446.

25. Chamkha AJ. Solutions for fluid-particle flow and heat transfer in a porous channel. *International Journal of Engineering Science* 1996; **34**:1423–1439.
26. Jean TH, Peddieson J. One-dimensional equations and solutions for particulate suspension flows. *International Journal of Engineering Science* 1997; **35**:803–818.
27. Apazidis N. On two-dimensional laminar flows of a particulate suspension in the presence of gravity field. *International Journal of Multiphase Flow* 1985; **11**:675–698.
28. Usha R, Prema K. Interaction of peristaltic transport of a particle-fluid suspension with Poiseuille flow. *Proceedings of ASME Fluid Engineering Conference*, vol. FED-237, San Diego, U.S.A., 1996; 753–760.
29. Usha R, Prema K. Interaction of pulsatile and peristaltic transport induced flows of a particle-fluid suspension. *Zeitschrift fiir Angewandte Mathematik und Mechanik* 1998; **78**:207–212.
30. Drew DA, Lahey RT. Phase distribution mechanisms in turbulent low-quality two-phase in a circular pipe. *Journal of Fluid Mechanics* 1982; **117**:91–106.
31. Sinclair JL, Jackson R. Gas-particle flow in a vertical pipe with particle–particle interaction. *American Institute of Chemical Engineers Journal* 1989; **35**:1473–1486.
32. Drew DA, Segal LA. Averaged equations for two-phase flows. *Studies in Applied Mathematics* 1971; **50**: 233–245.
33. Batchelor GK. Transport properties of two-phase materials with random structure. *Annual Review of Fluid Mechanics* 1974; **6**:277–285.
34. Batchelor GK. Diffusion of particles with hydrodynamics interaction. *Journal of Fluid Mechanics* 1976; **74**:1–29.
35. Zuber N. On the dispered flow in the laminar flow regime. *Chemical Engineering Science* 1964; **19**:897–903.
36. Saffman PG. The lift on a small sphere in a slow shear flow. *Journal of Fluid Mechanics* 1965; **22**:385–400.
37. Rubinow SI, Keller JB. The transverse force on a spinning sphere moving in a viscous fluid. *Journal of Fluid Mechanics* 1965; **11**:447–459.
38. Soo SL. Pipe flow of suspensions. *Applied Scientific Research* 1969; **21**:68–84.
39. Charm SE, Kurland GS. *Blood Flow and Micro-Circulation*. Wiley: New York, 1974.
40. Jager W, Mikelic A. On the roughness-induced effective boundary conditions for a viscous flow. *Journal of Differential Equations* 2001; **170**:96–122.
41. Achdou Y, Pironneau O, Valentin F. Effective boundary conditions for laminar flows over periodic rough boundaries. *Journal of Computational Physics* 1998; **147**:187–218.
42. Van Dyke M. *Perturbation Methods in Fluid Mechanics*. Parabolic Press: Stanford, CA, 1975.
43. Selvarajan S. Investigation of flow through wavy walled channels and its stability characteristics. *Ph.D. Thesis*, Department of Aerospace Engineering, Indian Institute of Technology Madras, Chennai, March 1998.
44. Scott MR, Watts HA. Computational solution of linear two-point boundary value problems via orthonormalization. *SIAM Journal on Mathematical Analysis* 1977; **14**:40.
45. Canuto C, Hussaini MY, Quarteroni A, Zang TA. *Spectral Methods in Fluid Dynamics*. Springer: Heidelberg, 1988.

